Grande Emilio (Orcid ID: 0000-0003-3995-0380)
Visser Ate (Orcid ID: 0000-0003-4048-4540)
Zimmer Margaret (Orcid ID: 0000-0001-8287-1923)

Title: Tidal frequencies and quasiperiodic subsurface water level variations dominate redox dynamics in a salt marsh system

Running title: Quasiperiodic groundwater levels dominate Eh dynamics in a salt marsh

Authors: Emilio Grande[1], Bhavna Arora[2], Ate Visser[3], Maya Montalvo[1], Anna Braswell[4], Erin Seybold[5], Corianne Tatariw[6], Kathryn Beheshti[7,8], and Margaret Zimmer[1]

[1] University of California Santa Cruz, Earth and Planetary Sciences
[2] Lawrence Berkeley National Laboratory, Energy Geosciences Division
[3] Lawrence Livermore National Laboratory, Nuclear and Chemical Sciences Division
[4] University of Florida, School of Forest Resources and Conservation, Fisheries and Aquatic Sciences Program
[5] University of Kansas, Kansas Geological Survey
[6] University of Alabama, Department of Biological Sciences
[7] University of California Santa Cruz, Ecology and Evolutionary Biology
[8] University of California Santa Barbara, Marine Science Institute

Corresponding Author: Emilio Grande.
Department of Earth and Planetary Sciences, University of California Santa Cruz, Santa Cruz, CA 95064. Email: emgrande@ucsc.edu

Abstract
Salt marshes are hotspots of nutrient processing en route to sensitive coastal environments. While our understanding of these systems has improved over the years, we still have limited knowledge of the spatiotemporal variability of critical biogeochemical drivers within salt marshes. Sea-level rise will continue to force change on salt marsh functioning, highlighting the urgency of filling this knowledge gap. Our study was conducted in a central California estuary experiencing extensive marsh drowning and relative sea-level rise, making it a model system for such an investigation. Here we instrumented three marsh positions subjected to different degrees of tidal inundation (6.7%, 8.9%, and 11.2% of the time for the upper, middle, and lower marsh positions, respectively), providing locations with varied biogeochemical characteristics and hydrological interactions at the site. We continuously monitored redox potential (Eh) at depths of 0.1, 0.3, and 0.5 m, subsurface water levels (WL), and temperature at 0.7 m depth at each marsh position. To understand how drivers of subsurface biogeochemical processes fluctuate across tidal cycles, we used wavelet analyses to explain the interactions between Eh and WL. We found that tidal forcing significantly affects key drivers of biogeochemical processes by imparting controls on Eh variability, likely driving subsurface hydro-biogeochemistry of the salt marsh. Wavelet coherence showed that the Eh-WL relationship is non-linear, and their lead-lag relationship is variable. We found that precipitation events perturb Eh at depth over timescales of hours, even though WL show relatively minimal change during events. This work highlights the importance of high frequency in situ measurements, such as Eh, to help explain factors that govern subsurface biogeochemistry and hydrological processes in salt marshes.
Keywords: Salt marsh hydrology, wavelet analysis, coastal hydrology, hydro-biogeochemistry

This article has been accepted for publication and undergone full peer review but has not been through the copyediting, typesetting, pagination and proofreading process which may lead to differences between this version and the Version of Record. Please cite this article as doi: 10.1002/hyp.14587

1- Introduction

Coastal wetlands are dynamic hydrologic systems where terrestrial groundwater, terrestrial surface water, and seawater mix. These systems play an important role in global biogeochemical cycles, promoting both carbon storage and nitrogen removal, in part due to the saturated conditions resulting from frequent inundation (Valiela and Cole, 2002; Giblin *et al.*, 2013; Reading *et al.*, 2017). Despite the importance of the dynamic hydrology in marshes, the bi-directional hydrologic interaction between terrestrial and marine sources is poorly understood.

Currently, one of the biggest impediments to developing robust water quality knowledge in coastal wetlands is an incomplete understanding of short-time dynamics and a lack of sampling at timescales over which nutrients are removed, retained, and transported. A first step towards improving this understanding is to determine the time scales at which surface-subsurface hydrologic interactions occur in salt marshes, as hydrologic forcing is likely an important driver of nutrient cycling and overall biogeochemistry (Guimond *et al.*, 2020b; Guimond and Tamborski, 2021). Documenting the current temporal variability of these interactions and associated nutrient concentrations will further aid in predicting future conditions in these dynamic coastal systems under a changing climate (Crotty *et al.*, 2020; Buffington *et al.*, 2021).

Available nutrients and other biogeochemical parameters in salt marshes are usually limited to synoptic, irregular sampling, or long-term but coarse resolution such as monthly time series (Reading *et al.*, 2017). Further, hydrologic forcing like storms and tidal inundation, which drive biogeochemical parameters, are short-lived, episodic events that may be missed by coarse resolution sampling. Although recent efforts have focused on measuring nutrient concentrations at high temporal resolution using sensors (Birgand *et al.*, 2016; Messer *et al.*, 2019; Liu *et al.*, 2020), these remain uncommon due to the difficulty and high costs associated with collecting these datasets. A promising solution to studying rapid temporal hydrological and biogeochemical variations in salt marshes is to use continuous *in situ* redox potential (Eh) measurements. Eh describes the energetic favorability of a reaction and indicates the dominant geochemical conditions or potential for carbon loss via oxidation. For example, high Eh values are indicative of aerobic or oxygenated conditions. *In situ* Eh measurements are comparatively easy and cheap to collect (Wallace *et al.*, 2019; Guimond *et al.*, 2020a), and using several probes can help capture the extensive spatial variability in salt marsh systems with respect to surface-subsurface hydrologic interactions.

Eh variability in salt marshes has been linked to sediment characteristics, temperature, and hydrologic forcing (Vorenhout *et al.*, 2004), but hydrology has been shown to be the most significant control on Eh as it is related to oxygen availability (Ensign *et al.*, 2008). This is because surface waters (or waters in contact with the atmosphere) have relatively high dissolved oxygen (DO) levels compared to subsurface water. DO is an important indicator of water pollution as it is critical for aerobic respiration (Boyd, 2000). Low DO levels are commonly found in wetlands as they are subjected to frequent submersion and contain abundant decomposing organic material (Hammer and Bastian, 1989; Steinmuller and Chambers, 2019; Orduña-Gaytán *et al.*, 2022). Further, previous work has shown that Eh can be an indicator of hydrological processes. Eh has been used to represent localized advective oxygen transport in forested wetlands as high Eh represents oxygen-rich flow paths (Lahiri and Davidson, 2020). Three-dimensional monitoring of Eh showed that high Eh conditions persist along high-permeability preferential flow paths where oxygenated surface water can easily flow in a shallow riparian aquifer (Wallace and Soltanian, 2021). Additionally, tidal inundation in coastal

environments were observed to have a strong relationship with denitrification rates and consequently Eh variations (Ensign *et al.*, 2008). Therefore, combining high-resolution *in situ* Eh measurements with inundation extent can be used to evaluate the frequency at which biogeochemical processes occur and the timescale at which pore water and subsurface water interact in these salt marsh systems.

Because biogeochemical processes in salt marsh pore water are complex, nonlinear, and rapid, changes to measured Eh can simultaneously signal the influence of multiple drivers, such as water level. Wavelet analysis has been shown to be useful for carrying out this timescale analysis of water chemistry parameters (Kumar and Foufoula-Georgiou, 1997; Arora *et al.*, 2016). Wavelet transform is used to decompose a time series signal into time and frequency domains simultaneously (Foufoula-Georgiou and Kumar, 1994; Torrence and Compo, 1998). Because of this capability of time-frequency localization, wavelet analyses can determine discontinuities, seasonal trends, and long-term patterns in the time series (Daubechies, 1992). For example, wavelet analysis has been used with diverse hydrologic parameters to study runoff generation in response to timing and magnitude of precipitation (Kantelhardt *et al.*, 2003; Partal, 2012). Wavelet transforms of temperature were also used to identify hotspots of submarine groundwater discharge (Henderson *et al.*, 2008). Moreover, this method has been used to understand redox dynamics and solute concentrations in a diversity of settings, from a municipal landfill site to a uranium-contaminated Department of Energy field site (Martínez and Gilabert, 2009; Arora *et al.*, 2013, 2016). In coastal environments, wavelet transform has been applied to periodic water quality measurements to assess the area's environmental health over several years (Venkatesh *et al.*, 2021). In addition, wavelets were used on continuous Eh data in a tidal river to assess hydrologic forcing on biogeochemistry over different timescales (Wallace *et al.*, 2019).

Given this technique's strengths and applicability, we use wavelet transform of continuous Eh and shallow subsurface water level measurements. To advance understanding of the spatiotemporal variability of hydrological and biogeochemical processes in coastal systems, we address the following questions:

1- Is there spatiotemporal variability at intra/intertidal scales in salt marsh subsurface hydrology and biogeochemistry?

2- What is the role of seasonal climatic factors, such as precipitation, for salt marsh biogeochemistry?

3- What are the drivers of redox conditions and their role in subsurface hydrology?

2- Methods

2.1 Site Description

This study was conducted at the Elkhorn Slough National Estuarine Research Reserve in Monterey, California (Figure 1A). The Mediterranean climate of Elkhorn Slough has pronounced wet/dry seasonal dynamics, which provide an ideal setting to understand the diel and seasonal variations in climatic forcing that impact subsurface inundation and biogeochemical conditions. During this study (Feb 2020-March 2021), air temperature varied between 0.3 ^{o}C and 35.4 ^{o}C, while water temperature ranged between 10.7 ^{o}C and 19.1 ^{o}C. Water levels were also variable, ranging between 0.57 m above the ground surface (during high tides, 2.17 m amsl) and 0.24 m below the ground surface (1.35 m amsl), reflecting the daily tidal inundations. Water levels during the study period had a mean, median, and standard deviation of 1.58 m amsl, 1.58 m amsl, and 0.09 m amsl, respectively. Total precipitation over the study period totaled 396.8 mm.

Our work focused on a 25 m experimental transect in an emergent wetland (Figure 1A, black star). The site was delineated into upper, middle, and lower marsh positions through elevation surveys and inundation extents (supporting information S1), with an elevation difference of 0.24 m over a 24 m profile (Figure 1D). The elevations above mean sea level of each marsh position are 1.79 m, 1.65 m, and 1.55 m for the upper, middle, and lower marsh, respectively. These elevations are inundated 6.7 %, 8.9 %, and 11.2 % of the time, respectively, based on water level data collected at the site between February 2019 and February 2021. These wetland positions coincide with previous delineations of salt marshes across the Elkhorn Slough estuary based on vegetation coverage by elevation (Woolfolk and Labadie, 2012), and thus, are representative of the estuary. Native pickleweed (*Salicornia pacifica*) dominates the marsh area (Van Dyke and Wasson, 2005), underlain by partially decomposed organic soils. For this study, we focus on temporal variations in Eh from these three locations that have distinct inundation regimes, vegetation activity/coverage, and micro-topography and that are representative of common/dominant landscape positions found across emergent wetlands at Elkhorn Slough.

We analyzed soil bulk density at depth in each marsh position at 0.05 m intervals (Figure 1B). The density measurements showed an increase in density from the surface down to 30 cm depth, where the bulk density was highest (Figure 1D). From 30 cm depth down to 50 cm, the bulk density of the soil decreased to values similar to the surface. Bulk density decreased from the upper marsh to the lower marsh position (Figure 1D).

We developed a network of co-located observation wells at each marsh position to study water fluctuations across the site (Figure 1D). We installed the wells to a depth of 0.7 m by pushing the PVC pipe directly into the ground to minimize gaps around the pipe, which could cause artificial water movement vertically along the well's annulus. The wells were screened from 0.05 m below the surface to the bottom of the well and water level and temperature were recorded with Solinst pressure transducer loggers (Ontario, Canada) at 5-minute intervals. Air pressure was also measured in the transect at 5-minute intervals to barometrically correct the water pressure measurements. For simplicity, the water level and temperature were averaged at hourly intervals.

We installed Eh probes (Paleo Terra, Amsterdam, Netherlands) next to each observation well (~1 m apart) to capture the range of Eh fluctuations over tidal and seasonal cycles and use them to indicate the possible dominant biogeochemical processes occurring at different time scales. The Eh probes consist of fiberglass-epoxy tubes embedded with an array of 3 platinum electrodes and a reference electrode filled with a potassium chloride solution used as a standard for the measurements (Figure 1C). Eh was measured at 0.1, 03, and 0.5 m depths below the ground surface (Figure 1D). Measurements were recorded at 1 min intervals between March 1st, 2020 and February 26th, 2021. We calculated the variance over the course of the study period for the Eh time series to control for measurement drifts. Similar to other data, these time series were also averaged to hourly intervals. Eh values were not corrected for pH. In addition, we installed a deep piezometer at 3.5 m below the surface in an upland location (in the same profile but ~8 m from the salt marsh, Figure 1B), with no influence from the daily tides. The piezometer was completed with a 0.15 m screen at the bottom. We continuously measured water level in this piezometer at 5 minute intervals to monitor fluctuations in the regional terrestrial groundwater level and evaluate the potential for fresh subsurface water to move laterally towards the salt marsh.

2.2 Ancillary Data

Eh is related to the concentration of different redox pairs in the soil, and oxygen is the first acceptor that plays a critical role in Eh variability (Vorenhout *et al.*, 2004). Although oxygen is introduced into the soil through diffusion and radial oxygen loss in the rhizosphere (Adema and Grootjans, 2003)(Koop-Jakobsen and Wenzhöfer, 2015). Thus, we expected that tidal processes (described above) and weather conditions would be the dominant drivers of Eh in the soil. To account for weather-driven oxygen inputs, we included hourly meteorological data, obtained from the Elkhorn Slough Meteorological Station (Figure 1A) in our study. The station is managed and maintained by the National Estuarine Research Reserve System (NERR, 2021). Our analyses used relative humidity, barometric pressure, precipitation, wind speed, total photosynthetically active radiation, and air temperature. These parameters associated with weather conditions have been observed to explain Eh variability in non-tidal inundated systems, mainly a paddy field (Minamikawa and Sakai, 2007) and also in waterlogged peats (Haavisto, 1974).

To further study the role of vegetation on Eh, we included hourly potential evapotranspiration (*ET*). *ET* was obtained from the California Irrigation Management Information System (CIMIS), which is maintained by the California Department of Water Resources (DWR). *ET* is estimated using the Penman-Monteith equation (Allen *et al.*, 1998). DWR manages a station within 5 km of our experimental transect (Station 129; 36.902779, -121.74193). CIMIS produces estimates of reference *ET* based on hydroclimatic data measured at their stations.

Monthly vegetation surveys were conducted across the experimental transect between October 2020 and September 2021. We used these surveys as a proxy to explore the potential controls of plant productivity on Eh. As mentioned above, pickleweed is the predominant marsh vegetation along our transect. Measurements of pickleweed canopy height, percent live cover, and percent total cover were made over two replicate 0.5 m by 0.5 m plots at each marsh position (n=6).

Considering that animal burrows directly affect salt marsh production, hydrology, and biogeochemistry (Crotty *et al.*, 2020; Guimond *et al.*, 2020a), we used monthly surveys of crab activity between October 2013 and August 2018 in Elkhorn Slough (Beheshti *et al.*, 2021) as a proxy for crab activity in our study. The crab activity study was conducted across the whole estuary and not limited to our transect. Further, crab counts were performed monthly. Therefore, these data were considered as a proxy for seasonal crab activity. *Pachygrapsus crassipes* is the dominant marsh crab in Elkhorn Slough (Beheshti *et al.*, 2022), with burrow densities often over 200 per m^2 in lower marsh positions (Beheshti *et al.*, 2022). Additionally, burrowing by *P. crassipes* has been shown to have a significant negative effect on bulk density and belowground biomass (Beheshti *et al.*, 2022). Evidence from a concurrent study showed that in the marsh interior, burrowing by P. crassipes hastens marsh recovery, likely due to improved drainage that ameliorate stressors associated with ponding, such as anoxia or sulfide toxicity (Beheshti et al. 2022). Total catch per unit effort (i.e., four pit-fall traps surveyed per 2 m by 1 m plot of marsh) were used to evaluate seasonal changes in crab activity and study their relationship with seasonal changes in Eh. Trapping data was conducted along the marsh edge of tidal creeks (n=5) that span from the mid to upper reaches of the estuary (Beheshti *et al.*, 2022).

3- Methodology

Redox reactions often show significant spatiotemporal variability (Vorenhout *et al.*, 2004, 2011; Guimond *et al.*, 2020a). High frequency Eh measurements can explain factors that govern subsurface biogeochemistry and hydrological processes in salt marshes. The use of principal component analysis, correlations, or other statistical techniques to examine biogeochemical data sets cannot always recognize the processes driving this variability as they lack the ability to incorporate temporal changes (Nezlin *et al.*, 2009).

In coastal systems affected by sea-level rise, there is a growing need to constrain biogeochemical processes to predict future scenarios (Ward et al., 2020). Continuous wavelet transform (CWT) is a promising tool for timescale analysis of water quality and hydrodynamics. CWT has been used to explain variabilities in water quality in coastal estuaries (Venkatesh et al., 2021). However, Venkatesh et al. (2021) used monthly samples of water quality, which allowed them to explain long-term variabilities, such as processes driving annual changes. The short-term variability of hydrological and biogeochemical processes, at time-scales over which nutrients are transformed, has been less studied. Recently, (Regier et al., 2021) used wavelet coherence on sub-hourly water level and salinity measurements to understand hydrologic connectivity between tidal creeks and floodplains in coastal systems. They found temporal variation in the lateral and vertical connectivity between the two, with neap tides controlling lateral connectivity, particularly during the dry season, and vertical connectivity dominated during spring tides. Our study uses a similar high-frequency measurement. However, in addition to improving our understanding of the hydrologic functioning of the shallow subsurface in the salt marsh, we linked the hydrologic processes to short-term variability in Eh. Here we explain variability in Eh, a key driver of biogeochemical processes, at time scales that can resolve the effects of tidal forcing in salt marsh subsurface hydrology and geochemistry. This application of CWT is significant as it can help identify potential control points, hot spots, and hot moments in marsh nutrient transformations. Therefore, the aim of the wavelet analyses was to 1) extract the complex linkages among biogeochemical drivers (e.g., Eh) and other environmental factors (e.g., subsurface hydrology); and 2) identify the temporal scales at which they exert dominant control using CWT, which has been found to be a powerful analytical tool (Alexander *et al.*, 2020).

3.1 Wavelet Analysis

As suggested above, we used wavelet analysis to analyze the measured Eh patterns and identify dominant scales of variability across the three studied marsh positions. In particular, we used multilevel decomposition to understand the hydrologic processes dictating patterns of biogeochemical drivers at different timescales.

3.1.1 Time-frequency processing

Wavelet transform is one of the most commonly used time-frequency analysis techniques for studying multiscale, nonstationary processes over spatial and temporal scales (Addison, 2005; Beecham and Chowdhury, 2010). CWT is obtained by decomposing the data $D(t)$ with a wavelet function $\psi(t)$ and creating wavelet coefficients W that designate the relationship among the wavelet function and the data:

$$W_D(a,b) = \int_{-\infty}^{\infty} \Psi^*_{a,b}(t) D(t) dt \quad (1)$$

where t is time, $*$ is the complex conjugate of the wavelet function, illustrated by:

$$\boldsymbol{\Psi_{a,b}(t) = \frac{1}{\sqrt{a}}\Psi(\frac{t-b}{a}), a > 0, -\infty < b < \infty} \quad (2)$$

where a is the scale parameter that determines the dilation or contraction, and b is the shift parameter that dictates the location of the wavelet. The flexibility of the wavelet to be stretched and translated in both time and frequency domains helps identify patterns across different time scales (Kumar and Foufoula-Georgiou, 1997). The wavelet must satisfy three central properties:

1- zero mean, $\int_{-\infty}^{\infty} \Psi(t)dt = 0$;

2- unit energy, $\int_{-\infty}^{\infty} \Psi^2(t)dt = 1$;

3- conservation of energy during transformation (Daubechies, 1992).

Several wavelet functions have been described in the literature. Here, we used the Morlet wavelet to derive the dominant frequencies from the Eh time series data. The Morlet wavelet is suitable for feature extraction because it is well localized in space and time (Grinsted *et al.*, 2004), and it has been used in similar datasets (Arora *et al.*, 2013; Wallace *et al.*, 2019; Venkatesh *et al.*, 2021). This wavelet has complex and real elements and facilitates identifying and fine-tuning the significant frequencies (Hariprasath and Mohan, 2008).

3.1.2 Local and Global Wavelet

The modulus of the wavelet coefficient is applied to produce a continuous-time power spectrum $p_D(a,b)$ described as:

$$p_D(a,b) = W_D(a,b)W_D^*(a,b) = |W_D(a,b)|^2 \quad (3)$$

This wavelet power spectrum is helpful as it produces the time-series variance in the frequency and time domains (Guan *et al.*, 2011). The global wavelet can be obtained by calculating the mean of the local power spectrum along the time axis (Torrence and Compo, 1998):

$$\underline{W}^2(a,b) = \frac{1}{N}\sum_{n=0}^{N-1}|W_D(a,b)|^2 \quad (4)$$

where N is the length of the time-series. We calculated a 95% confidence level for the global wavelet spectrum and the significance interval of the contours in the local wavelet, with a significance testing on the background spectrum. Following (Torrence and Compo, 1998), the distribution of the local wavelet at each time t and scale a is given as:

$$\frac{|W_D(a,b)|^2}{\sigma^2} \Rightarrow \frac{1}{2}P_k\chi_2^2 \quad (5)$$

In (5), χ^2 is the chi-square value obtained for the 95% confidence level, σ^2 is the variance, and P_k is the mean spectrum at the Fourier frequency k that corresponds to a. We used a red-noise background spectrum, which is obtained as (Torrence and Compo, 1998):

$$P_k = \frac{1-\alpha^2}{1+\alpha^2-2\alpha cos(2\pi k/N)} \quad (6)$$

where P_k is the background spectrum for red-noise, k (= 0 … N/2) is the frequency index, and α is an assumed lag-1 autocorrelation. A 95% significance level for the global wavelet was also calculated using a red-noise background spectrum. The spectrum of the global wavelet can also be fitted by a chi-square distribution of the form $\frac{\chi_v^2}{v}$, where v (the degree of freedom) is calculated as (Torrence and Compo, 1998):

$$v = 2\sqrt{1+(\frac{t_{avg}\delta t}{\gamma a})} \quad (7)$$

In (7), t_{avg} is the number of points averaged over, γ is the empirically calculated decorrelation factor for the mean power across the time axis, and δt is the sampling frequency. We used the R software (R Core Team, 2019) package Biwavelet (Gouhier *et al.*, 2021) for calculating the wavelet spectrums and the confidence intervals. We represented the edge effects of time-frequency (Guan et al., 2011) with a cone of influence, illustrated by the shaded region in the wavelet power spectrum (e.g., Figure 3), and omitted it from the analysis.

3.1.3 Wavelet Coherence

Wavelet coherence analysis can explain the relationship of two time series in the time-frequency domain. The correlation between the wavelet power of two variables (*D1, D2*) can be quantified through wavelet coherence analysis (Grinsted *et al.*, 2004):

$$p_{D1,D2}(a,b) = W_{D1}(a,b)W_{D2}^{*}(a,b) \quad (8)$$

The wavelet coherence may be decomposed into modulus $p_{D1,D2}(a,b)$ and phase $\Phi_{D1,D2}(a,b)$ as (Maraun and Kurths, 2004):

$$p_{D1,D2}(a,b) = \left|p_{D1,D2}(a,b)\right| e^{i\Phi_{D1,D2}(a,b)} \quad (9)$$

In (9), the modulus quantifies the power and the phase describes the lag in time between *D1* and *D2*. We used wavelet coherence to study how Eh and other non-stationary variables, specifically subsurface water level, varied in time.

We used arrows to represent the lead-lag relationship between Eh and subsurface water level. Arrows pointing to the left symbolize that the two time series are anti-phase (there is a difference of phase between the two signals of π (or -π), that is to say, the two waves have opposite signs and for example a high in subsurface water level corresponds to a low in Eh). Arrows pointing towards the right indicate that the time series are in phase (both series move in the same direction). When the arrows point down, the water level is leading (e.g., a high in subsurface water level occurs earlier than a high in Eh). When the arrows point upwards, the Eh time series leads the water level.

3.1.4 Multilevel Decomposition of Redox potential

The multilevel decomposition (MLD) allows decomposition of a time series into a number of frequency bands at discrete levels of time scales. At the first step, the time series data is split into two, yielding the high-pass bandwidth (i.e., detailed components), and the low-pass bandwidth (i.e., approximate components; (Quiroz *et al.*, 2011). Each low-pass bandwidth can continue to be decomposed to achieve the next level of hierarchy. This methodology, therefore, allows removing the noise (detailed components) and recovering the data's smoothed trend (approximate components) for each level. The decomposition levels are based upon the sampling frequency and the total length of the time series (Mallat, 1999). The detailed and approximation components are determined by iteratively using a high-pass filter and an associated low-pass filter, which requires satisfying orthonormality (Labat *et al.*, 2004). A wavelet function $\psi(t)$ composes the high-pass filter in the wavelet transform, and its scaling function $\phi(t)$ determines the low-pass filter. The detailed (D_m) and approximation (A_m) components at a given decomposition level m can be calculated as:

$$D_m(t) = \sum_{k=-\infty}^{\infty} W(m,k)\psi_{m,k}(t) \quad (10)$$

$$A_m(t) = \sum_{k=-\infty}^{\infty} S(m,k)\phi_{m,k}(t) \quad (11)$$

where S is the scaling coefficient and k is a discrete location index. We used the Daubechies 5 (Db5) wavelet and scaling function, which meets the orthogonality requirement.

The approximation and detailed coefficients follow powers of two (i.e., dyadic sampling) to capture the natural frequencies of the Eh data set at 2, 4, 8, 16, and 32-hour scales, respectively. Although frequencies of interest (e.g., tidal frequencies) would be observed at ~12 and ~24-hour scales, these dyadic decomposition levels offer an opportunity to investigate the intertidal cycles seen in the salt marsh. We studied the 16 h approximation component variability and its relationship with other environmental parameters available for this study (see section 2.2). Specifically, we zoomed in around the largest precipitation event of the studied period to estimate the effects of precipitation as a driver of Eh. We used the Wavelet Toolbox from MatLab (The MathWorks, 2021) to obtain the MLD.

3.2 Mutual Information

In order to identify the key factors causing temporal variability in the Eh data, we chose to employ mutual information. The mutual information of two random variables quantifies how much information is obtained about one variable by observing the other variable. Unlike the correlation coefficient, mutual information is not limited to linear dependence (Brunel *et al.*, 2010; Zhang *et al.*, 2012). Mutual information is more comprehensive and defines how different the joint distribution of the two variables (X, Y) is from the product of the marginal distributions of X and Y (Shannon and Weaver, 1949):

$$I(X;Y) = D_{KL}(P_{(X,Y)} || P_X \otimes P_Y) \quad (12)$$

where X and Y are random variables (e.g., Eh, water level) with values in the $X \times Y$ space, marginal distributions P_X and P_Y, and join distribution $P_{(X,Y)}$. D_{KL} is the Kullback-Leibler divergence (i.e., reactive entropy, (Cover and Thomas, 2006)). In our study, we used mutual information analysis between Eh and *ET,* subsurface water level in each marsh position, subsurface water temperature in each marsh position, terrestrial groundwater level, precipitation, and the rest of environmental parameters described in section 2.2

In mutual information, the null hypothesis is that $I(X; Y)=0$ (i.e., the two signals are independent). To test the statistical significance of the analysis, we used an equal variance t-test, which is valid for large samples from non-normal distributions and can be used when both data sets consist of the same number of samples and it has been used to test the statistical significance of mutual information analysis (Sarkar and Pandey, 2020). We used a one-tailed test with significance level $\alpha = 0.0001$, which corresponds to a confidence level of ~99.9%.

Further, we normalized $I(X;Y)$ to scale the results between 0 (no mutual information) and 1 (perfect correlation). The normalization uses the entropy $H(X)$ of each individual signal, and can be calculated as (Kvålseth, 2017; Zbili and Rama, 2021):

$$NMI(X;Y) = \frac{I(X;Y)}{\sqrt{H(X)*H(Y)}} \quad (13)$$

And $H(X)$ of the discrete random variable X is calculated from its probability ($P(x)$) and surprise ($logP(x)$) as:

$$H(X) = -\sum_{i=1}^{n} P(x_i) logP(x_i) \quad (14)$$

4- Results

4.1 Redox potential patterns in the spatiotemporal domain

There was considerable spatial and temporal variability in Eh across marsh positions and with depth at our salt marsh transect (Figure 2, supporting information S2). Furthermore, anaerobic conditions (Eh < 250 mV; (Søndergaard, 2009)) dominated the area over the study period across all marsh positions. Eh increased significantly with elevation, with median values

of -421 mV, -404 mV, and -377 mV at the lower, middle, and upper marsh positions, respectively (Kruskal-Wallis test: $H=9699.3$, $df = 2$, $p < 0.001$). Additionally, median Eh values varied significantly between 10 (median = -387 mV), 30 (median = -424 mV), and 50 cm depths (median = -407 mV) (Kruskal-Wallis test: $H=19639$, $df = 2$, $p < 0.001$).

Median Eh was highest at 10 cm and lowest at 30 cm, and this is consistent across the entire measurement period (Figure 2). At 10 cm, especially during the wet season (i.e., November-January), the oxygen delivery and consumption processes are readily seen in the Eh profiles (Figure 2). During this period, we observed the highest range of Eh values. At all marsh positions, Eh is relatively lower at 30 cm than at 50 cm, except for the middle marsh, where the Eh measurements at 50 cm were consistently lower, suggesting that Eh doesn't continuously decrease with depth but rather is likely related to soil properties, such as bulk density (Figure 2, S3). Further, throughout the monitoring period, measurements at the 50 cm depth remained somewhat spatially and temporally constant (~ -400 mV), highlighting the lower Eh variability at depth in salt marsh sediments.

4.2 Redox potential patterns in the time-frequency domain

We studied the temporal variability in Eh as a result of tidal fluctuations using the Morlet wavelet (Figure 3). Based on the Morlet wavelet, all marsh positions and depths studied show dominant powers at periods of 12 h and 24 h (areas marked with black polygons in the CWT, or with powers above the red dashed line in the global wavelet spectrum, which mark the 95% confidence level, Figure 3). The significant powers at the 12 and 24 h periods coincide with the sub-daily and daily tidal frequencies (Taniguchi, 2000), suggesting a relationship between the water level in the salt marsh (i.e., inundation extents) and Eh measurements.

At 10 cm depth, significant powers at specific tidal frequencies (12 and 24 h periods in Figure 3, Table 1) are seasonal; significant powers start in August 2020 and stop during the winter months. The significant powers start earlier in the upper and middle marsh than at the lower marsh position. In addition to significant powers at (sub)daily tidal cycles, the CWT of the 10 cm probes showed significant powers at larger periods of ~708 h (29.5 days) and ~355 h (14.8 days), corresponding with the lunar cycles (Figure 3; (Taniguchi, 2000)). However, significant powers at these frequencies are not observed at other depths.

At 30 cm, Eh measurements showed different patterns in the CWT across marsh positions. In the upper marsh position, the CWT shows significant powers at 12 and 24 h periods continuously from April through October 2020. The middle marsh position showed significant powers for a limited time (predominantly in summer, Figure 3, Table 1), and only the ~24 h period is significant in the global wavelet. In the lower marsh position, Eh displayed significant powers at tidal frequencies (~12 and ~24 h periods) throughout the studied period (Figure 3). No lunar cycle frequencies are observed at this depth.

The CWT of Eh at 50 cm displayed temporal and spatial variability. In the upper marsh, Eh measurements show significant powers at tidal frequencies only during some days in May, July and August 2020 (Figure 3). However, in the middle marsh position, significant powers at tidal frequencies show a gap between July and August 2020. During that period, the middle marsh showed significant powers at frequencies associated with the lunar cycle (Figure 3, Table 1). The lower marsh position also showed a gap in the significant powers of tidal frequencies, however the gap started in June and ended in October 2020.

4.3 Controlling Processes

Based on the mutual information analysis, regional terrestrial groundwater level, subsurface water temperature and subsurface water level in the salt marsh share the most information with Eh, with normalized mutual information (NMI) of 0.99, 0.98, and 0.97, respectively (Figure 4).These parameters are followed by air temperature and total PAR, wth NMI of 0.71 and 0.63, respectively (Figure 4). Precipitation and Eh share low mutual information, with NMI of 0.03 (i.e., these two time series are somewhat independent). Here, we illustrate the results from the mutual information analysis only for the lower marsh position, but other marsh positions had similar results (S4).

The temporal variability of the 16 h approximation coefficients was graphically compared with the most significant parameters from the mutual information analysis to identify and temporally separate the processes affecting Eh's dominant frequencies (Figure 5). Here, we zoom-in to show data between January 20th and February 10th 2021, corresponding to dates around one of the few precipitation events of the 2021 water year in the area (Figure 5). The precipitation event totaled 147.6 mm in 3 days with a maximum intensity of 11.2 mm/h. During this focal period, Eh and ET were out of phase (Figure 5A). ET ranged between 0 and 0.8 mm/h, with a mean, median, and standard deviation of 0.13 mm/h, 0.1 mm/h, and 0.2 mm/d, respectively. The maximum daily Eh value occurred at times of minimum ET (at night). Subsurface water temperature displayed a relatively low temporal variability, contrasting with air temperature values for the site, as would be expected (Figure 5B).

During the period shown in Figure 5, the lead-lag relationship between subsurface water level and Eh is observed to be variable. For example, the maxima in water level and Eh are in phase in the first two days, but the two variables are out of phase for the remaining period. The regional terrestrial groundwater level varied (i.e., increased) rapidly in response to precipitation events (Figure 5B). Over the whole study period, the water table fluctuated between 1.77 m amsl (in the dry summer and fall season) and 2.78 m amsl (in the wet winter season, S5), with a mean, median, and a standard deviation of 2.23 m amsl, 2.19 m amsl, and 0.30 m amsl, respectively. The regional terrestrial groundwater level is generally higher than the subsurface water level in the salt marsh. The regional terrestrial groundwater level is only lower than the subsurface water level during king tides in very dry periods (S5).

Note that the detailed components (d1, d3, d3, d4, and d5) represent the "noise" in data at each scale and were therefore removed from the analysis. This can be further confirmed from Figure 5C where the detailed components are damped during the precipitation event, and amplified otherwise.

4.4 Wavelet Coherence

Overall, the results of Eh's mutual information and spectral analysis suggest that water level (i.e., tidal inundation) is a critical control in the temporal variability of Eh. In order to further describe the relationship between water level and Eh in the frequency space, wavelet coherence was performed. Here we show the power (modulus) and the phase (angle) for the wavelet coherence between water level and Eh at 30 cm in the lower marsh (Figure 6). The wavelet coherence for all other water levels and Eh comparisons showed similar behavior (S6).

Eh and subsurface water levels were significantly coherent at ~12 h and ~24 h periods across most of the studied period (power > 0.8 mV^2 in Figure 6). The frequency of high powers

(blue color in Figure 6) at tidal periods suggests a quasi-periodic relationship between Eh and subsurface water level. We also observed significant coherence at lunar cycles (14.8 and 29.5 days) over some periods, although more sporadic than the significant powers at tidal periods.

The phase plot (Figure 6) showed that the lead-lag behavior of the Eh and subsurface water level signals was not consistent throughout the studied period. The colors (blue) highlight when the two signals are in phase. We observed that Eh and water levels were in phase during lunar cycles and sporadically at tidal frequencies (shown by a phase of 0 radians, Figure 6). During other periods, we observed that the signals were anti-phase (shown by phases of -3 and +3 radians, Figure 6) at tidal periods. The arrows indicate that the subsurface water level leads Eh at lunar cycles and only at times for tidal periods. Nevertheless, the wavelet coherence showed a direct relationship between these two variables at tidal frequencies (12h and 24h), suggesting a relative change in the Eh time series across tidal cycles.

5- Discussion

5.1 Intertidal processes: Implications for the local hydrology

Tidal signals were observed in the Eh time series across all depths, suggesting that water level fluctuations influence Eh values in the salt marsh sediment. This was confirmed by CWT analysis that showed that Eh changed at tidal frequencies (even at depth; Figure 3), implying that tidal surface water interacts with pore water during high tide periods, allowing for some degree of exchange in water chemistry at these frequencies (12 and 24 h).

One potential mechanism that may explain rapid water movement through the salt marsh is filling of pores during high tides and evapotranspirative loss during low tides (i.e., water removed from the salt marsh sediment via ET). However, if this were the only mechanism acting in the Eh, we would likely observe strong seasonality in Eh, highlighted during the summer growing season, when ET is higher, which we did not see (e.g., Figure 3). Pickleweed, the predominant plant in the salt marsh, can have a rooting depth of over 0.5 m (Meinzer, 1927)

A second potential mechanism that may explain rapid water movement through the subsurface involves animal burrows. Animal burrows are abundant in these environments (S7) and favor pore water-tidal water exchange (Tait et al., 2016; Taillardat et al., 2019). Tidal water circulation through burrows was the 'engine' of water and solute exchange in a mangrove-dominated marsh (Stieglitz et al., 2013). Stieglitz et al. (2013) used Radon and Radium isotopes to calculate water balance fluxes, determining that water flushed through animal burrows accounted for 20% of the total annual river discharge in a watershed in the Great Barrier Reef, northeastern Australia.

Our observations also agree with Breier et al. (2009), who used Radium isotopes to explain the subsurface hydrology in the Elkhorn Slough estuary. They suggested a relatively fast turnover between inundation and drainage of tidal zones of subsurface water, though their model could not reproduce intertidal changes. Considering that the compressibility of water is very low (Fine and Millero, 1973; Osif, 1988), and because the salt marsh is saturated most of the time, more water cannot be added to the soil without removing some water (Wong *et al.*, 2009). This condition indicates a relatively high hydraulic conductivity and relatively fast circulation of pore water through the salt marsh platform. The exchange of this more oxygenated surface tidal water with pore water would lead to tidal variations in the Eh time series, highlighting the Eh-subsurface water level relationship. This process is complex and non-linear, with Eh and subsurface water levels displaying periodic changes in their lead-lag relationship (Figure 6).

5.2 Seasonal processes: Climatic forcing effects on salt marsh hydrology and biogeochemistry

The effect of precipitation in the salt marsh's subsurface water level was evident during our study. Although the tides primarily drive subsurface water level, the salt marsh drains between high and low tides (i.e., the water level is below the salt marsh surface, gray dashed line in Figure 5B, before the focal rain event). However, the salt marsh platform stays saturated after precipitation events, even during low tides, possibly due to the hydrologic forcing of the elevated terrestrial groundwater level. This observation suggests that precipitation water, and the corresponding increase in the terrestrial groundwater level (Figure 5 B), play a role in maintaining the subsurface water level elevated in the salt marsh. This implies that high antecedent moisture conditions, interpreted as periods of higher terrestrial groundwater levels, reduce the aeration of the salt marsh platform's top centimeters, unlike periods in which the salt marsh drains. This process has important implications for carbon retention as marsh draining might enhance carbon loss from the marsh sediments due to increased carbon oxidation (Guimond *et al.*, 2020a). On the other hand, aeration of salt marsh sediments enhance pollutant removal rates as oxygenation can increase biogeochemical processes, including decomposition of excess nutrients (Nivala *et al.*, 2020).

Seasonally, the influence of different water sources (e.g., precipitation, tidal surface water) and antecedent moisture conditions on Eh varied, and the use of MLD helped detect these changes (Figure 5). Using the approximation component , we identified changes in the Eh behavior during precipitation events. During rainless periods, we observed the effects of tidal forcings on the Eh approximated coefficient (Figure 5A). However, the tidal frequency is muted during precipitation events, and the Eh signal becomes relatively flat (Figure 5A). We observed this phenomenon at all depths and marsh positions studied. This process shows that precipitation water, which has a different chemical signature from tidal water, exchanges with the marsh pore water relatively fast after the onset of precipitation, and this is registered in the Eh measurements (Figure 5A).The effect of precipitation in the Eh record might be explained by increased lateral flow of fresh terrestrial groundwater from increased terrestrial groundwater levels during precipitation events (Figure 5). Although the study design does not test the specific mechanism of precipitation effects on Eh, the lateral flow of fresh groundwater across shallow subsurface marsh zones could also be driven by differences in density between fresh groundwater over saline marsh water. Additionally, direct, vertical infiltration of precipitation water into the salt marsh could be a significant factor. However, at the time scale used in this analysis (one year of hourly data), the mutual information cannot detect information that does not occur frequently, such as precipitation. More extended time series and coarser frequencies might show the effects of precipitation on Eh.

Seasonal changes in the terrestrial groundwater level and subsurface temperature variations at all marsh positions also drive subsurface Eh, as suggested by the mutual information analysis (Figure 4). The lateral flow of groundwater and its effect on subsurface water levels in salt marshes have been considered in the scientific literature. For example, (Menció *et al.*, 2017) used major ions, nutrients and water stable isotopes to study the hydrogeological dynamics of a salt marsh, also in a Mediterranean climate in Catalonia, Spain. They found that groundwater contributions to the salt marsh were significant, and played an important role in controlling water salinity. (Xie *et al.*, 2019) studied the importance of precipitation on salt marsh vegetation. They showed that post-dry season precipitation enhanced seedling establishment by influencing the suitability of abiotic factors for species niches. At the

same time, they found that plant–soil–rainfall interactions were nonlinear and likely controlled by tidal inundation. These studies highlight the important role of fresh groundwater-saline tidal water exchanges for salt marsh ecosystems. Our analysis shows that these interactions are present in our field site and that they influence Eh conditions in the subsurface.

Notably, the mutual information analysis showed that the terrestrial groundwater level and Eh are closely related. This relationship is likely due to similar factors affecting both signals. For example, tidal forcing, which is more evident in the Eh time series, but can impart slight variations in the terrestrial groundwater in coastal ecosystems (Turner *et al.*, 1997) (Abarca *et al.*, 2013).

5.3 Redox conditions, drivers, and subsurface hydrology

In our study, anoxic conditions dominated the transect with subtle Eh variations across most marsh positions. The redox conditions suggest that denitrification rates in the subsurface are substrate limited, with rapid consumption of nitrate occurring when nitrate is available. Previous studies at Elkhorn Slough have found that anthropogenic nitrate inputs are removed by denitrification in salt marsh sediments (Wankel *et al.*, 2009, 2011). In systems such as Elkhorn Slough that receive high loads of anthropogenic inorganic nitrogen (Chapin et al., 2004), this reinforces the idea that salt marshes are important modulators of water quality. Furthermore, despite strong variability in atmospheric forcing (e.g., precipitation), we observed relatively subtle seasonal fluctuations in Eh, suggesting that the capacity of the marsh to rapidly remove nutrients delivered from surface water is consistent throughout the year and may exert an impact on surface water quality year-round.

Sediment bulk density likely plays an essential role in controlling Eh variability in the sediment profile. Our analysis observed an overall decrease in mean Eh at each marsh position with increased soil density (S3). However, the relationship between Eh and bulk density varied between marsh positions, perhaps due to several parameters simultaneously influencing Eh (e.g., hydrology, climate, biotic processes). The most significant ranges in Eh values were observed closest to the sediment-water interface, and also, above the higher density, less permeable layer observed at the 30 cm depths across marsh positions (Figure 1D). This high-density layer likely reduces vertical oxygen transport during tidal inundations (Haberer *et al.*, 2014), resulting in episodic steep vertical redox gradients (Figure 2).

Marsh elevation is also a likely driver of spatial variability in Eh due to difference in inundation extent across the marsh platform. Although the differences in inundation extent across the marsh positions are relatively small (S1), we found that the less inundated upper and middle marshes were less reducing overall as is evidenced by the higher average Eh values (Figure 2). This illustrates the importance of tidal inundation, including the duration of the inundation event, for salt marsh biogeochemistry. Specifically, tidal forcing can drive whether nitrate is removed or retained by regulating oxygen and substrate delivery to sediments (Zheng *et al.*, 2016). Theelevational differences in Eh measured in our study could potentially impact marsh function by influencing the dominant microbial metabolic pathways (Falkowski *et al.*, 2008). Oxygen penetration into anoxic sediments promotes nitrification at relatively short timescales (Petersen *et al.*, 1994; Hamersley and Howes, 2005) as an electron acceptor stimulating denitrification. However, if sediments are more consistently reduced, such as at the low marsh position, sulfide accumulation can inhibit nitrification-denitrification coupling and instead promote nitrogen retention through dissimilatory nitrate reduction to ammonium (DNRA) (Joye and Hollibaugh, 1995; Murphy *et al.*, 2020). While we did not measure

biogeochemical transformations in this study, our finding that Eh differs between marsh elevations is particularly significant given that sea level rise will result in more frequent inundation of the upper marsh, potentially transforming its functionality to mirror the current lower marsh.

Overall, tidal inundation of the transect seems to be the dominant control on subsurface Eh across the salt marsh. Oscillatory tidewater and pore water interact within the marsh sediment, likely transporting oxygen and other electron acceptors to depth. Advective transport distances across tidal cycles are likely small, though this may depend on season. However, the continuing influence of oscillatory tides could heighten solute dispersion, causing a shallow vertical redox gradient that shifts somewhat over each tidal cycle (Wallace et al., 2019). The corresponding oscillations in Eh vertical gradients across positions have implications for the timing of nutrient removal and fluxes to coastal environments in salt marshes. Cyclic inundation and draining of pore water due to tidal forcing (or tidal pumping) can attenuate excess nutrients and have important water quality implications.

6- Conclusion and Implications

Biogeochemical parameters such as nutrients are commonly measured at monthly frequencies in coastal estuaries but significant nutrient processing can occur rapidly at much shorter time scales (e.g., precipitation events, tidal cycles). This study investigated the variability of Eh, a critical driver of biogeochemical processes, at time scales that can explain intertidal and intratidal variations. Further, because Eh is linked to moisture conditions, we studied the local subsurface hydrology of a salt marsh using continuous, high-frequency water level measurements. Our work shows that the subsurface hydrology is likely dynamic with the potential for tidal surface water to exchange with subsurface water at intra-tidal time scales (12 and 24 h periods). This observation highlights the necessity to measure analytes of interest at higher frequencies to explain the critical biogeochemical processes dominating coastal ecosystems.

Moreover, our analysis shows that precipitation water mutes the tidal signal observed in the Eh time series, indicating that precipitation disturbs subsurface Eh. This result implies a relatively fast exchange of precipitation water with pore water in the salt marsh. We hypothesize that the presence of crab burrows, which are abundant in these types of environments, allows for rapid pore water-surface water exchange at sub-hourly intervals. However, temporal changes in the lead-lag relationship between Eh and subsurface water level suggest that the relationship between these parameters is not linear, and instead influenced by many interlinked processes, such as terrestrial water levels, subsurface water temperature in the salt marsh, plant activity, etc.

Continuous wavelet transforms revealed that salt marsh subsurface Eh varies significantly at frequencies corresponding to lunar cycles (14.8 and 29.5 days). During periods of higher tides, the surface water-pore water exchange seems to be accentuated. A future research question would focus on studying the biogeochemical impacts of the lunar cycles on coastal systems.

Continuous measurements of Eh at high resolution over long periods enable understanding the variability and instantaneous effects of hydrologic forcing (e.g., precipitation events, tidal flooding) in the pore water chemistry of the salt marsh platform. Furthermore, high-resolution measurements permit signal analysis in the frequency domain. By implementing techniques like those shown here in continuous Eh data sets, subsurface conditions can be further studied by analyzing specific frequencies that explain the temporal variability of a time series. For example, wavelet analysis can aid in understanding subsurface hydrologic fluctuations as it can show the

effects of the tides in the subsurface or highlight the changes in the time series frequency when other water sources are present (e.g., precipitation water). Further, wavelet analysis can help understand reactive transport of Eh-sensitive solutes (e.g., nitrate), particularly in dynamic environments such as coastal estuaries.

As global climate shifts, factors including sea-level rise will induce changes in marsh position functioning and the services they provide. We used a relatively simple and robust methodology for evaluating key marsh processes. The methods presented here can assist in interpreting coastal processes, which can help with the urgency to predict future scenarios under sea-level rise conditions. Further, the application of these techniques have transformative influences on our knowledge of coupled hydrological and biogeochemical processes in marsh ecosystems.

Acknowledgement: The authors sincerely thank Dan Sampson from the University of California Santa Cruz for his valuable help programming and installing the electronic devices used in this study. We would also like to thank Andria Greene and Loren Tolley-Man for field assistance. We also thank John Haskins and the rest of the Elkhorn Slough National Estuarine Research Reserve for all their help and assistance throughout this study. EG was partially funded by a Cota-Robles fellowship through the University of California Santa Cruz, and by a Margaret A. Davidson fellowship (NA20NOS4200122). We acknowledge support from the DOE SBR NITRATES Project, funded by the U.S. Department of Energy, Office of Science, Office of Biological and Environmental Research, award number: DE-SC0021044. We acknowledge support from a California SeaGrant under California Natural Resources Agency Award Number C0303100. We thank Dr. Rebecca Barnes and one anonymous reviewer for their thoughtful comments and suggestions that have greatly improved the quality of this manuscript.

Conflict of Interest

The authors declare no conflict of interest.

Data Availability System

The data that support this manuscript are openly available in ESS Dive at ess-dive-41a0203a1aa8fe0-20220219T180403607

The codes to replicate the continuous wavelet transform, the global wavelet, the wavelet coherence and the multilevel decomposition are available at https://github.com/emgrande/WaveletAnalysis_ElkhornSlough_CA

7-References

Abarca E, Karam H, Hemond HF, Harvey CF. 2013. Transient groundwater dynamics in a coastal aquifer: The effects of tides, the lunar cycle, and the beach profile. *Water Resources Research* **49** (5): 2473–2488 DOI: 10.1002/wrcr.20075

Addison PS. 2005. Wavelet transforms and the ECG: a review. *Physiological Measurement* **26** (5): R155-199 DOI: 10.1088/0967-3334/26/5/R01

Adema EB, Grootjans AP. 2003. Possible positive-feedback mechanisms: plants change abiotic soil parameters in wet calcareous dune slacks. *Plant Ecology* **167** (1): 141–149 DOI: 10.1023/A:1023947411605

Alexander AC, Levenstein B, Sanderson LA, Blukacz-Richards EA, Chambers PA. 2020. How does climate variability affect water quality dynamics in Canada's oil sands region? *Science of The Total Environment* **732**: 139062 DOI: 10.1016/j.scitotenv.2020.139062

Allen R, Pereira L, Raes D, Smith M. 1998. Crop evapotranspiration-Guidelines for computing crop water requirements, FAO

Arora B, Dwivedi D, Hubbard SS, Steefel CI, Williams KH. 2016. Identifying geochemical hot moments and their controls on a contaminated river floodplain system using wavelet and entropy approaches. *Environmental Modelling & Software* **85**: 27–41 DOI: 10.1016/j.envsoft.2016.08.005

Arora B, Mohanty BP, McGuire JT, Cozzarelli IM. 2013. Temporal dynamics of biogeochemical processes at the Norman Landfill site: Temporal Dynamics at the Norman Landfill Site. *Water Resources Research* **49** (10): 6909–6926 DOI: 10.1002/wrcr.20484

Beecham S, Chowdhury RK. 2010. Temporal characteristics and variability of point rainfall: a statistical and wavelet analysis. *International Journal of Climatology* **30** (3): 458–473 DOI: 10.1002/joc.1901

Beheshti K, Endris C, Goodwin P, Pavlak A, Wasson K. 2022. Burrowing crabs and physical factors hasten marsh recovery at panne edges. *PLOS ONE* **17** (1): e0249330 DOI: 10.1371/journal.pone.0249330

Beheshti KM, Wasson K, Angelini C, Silliman BR, Hughes BB. 2021. Long-term study reveals top-down effect of crabs on a California salt marsh. *Ecosphere* **12** (8): e03703 DOI: 10.1002/ecs2.3703

Birgand F, Aveni-Deforge K, Smith B, Maxwell B, Horstman M, Gerling AB, Carey CC. 2016. First report of a novel multiplexer pumping system coupled to a water quality probe to collect high temporal frequency in situ water chemistry measurements at multiple sites: High-Resolution Water Chemistry in Time and Space. *Limnology and Oceanography: Methods* **14** (12): 767–783 DOI: 10.1002/lom3.10122

Boyd CE. 2000. Dissolved Oxygen and Redox Potential. In *Water Quality: An Introduction*, Boyd CE (ed.).Springer US: Boston, MA; 69–94. DOI: 10.1007/978-1-4615-4485-2_5

Brunel H, Gallardo-Chacón J-J, Buil A, Vallverdú M, Soria JM, Caminal P, Perera A. 2010. MISS: a non-linear methodology based on mutual information for genetic association studies in both population and sib-pairs analysis. *Bioinformatics* **26** (15): 1811–1818 DOI: 10.1093/bioinformatics/btq273

Buffington KJ, Janousek CN, Dugger BD, Callaway JC, Schile-Beers LM, Sloane EB, Thorne KM. 2021. Incorporation of uncertainty to improve projections of tidal wetland elevation and carbon accumulation with sea-level rise. *PLOS ONE* **16** (10): e0256707 DOI: 10.1371/journal.pone.0256707

Cover TM, Thomas JA. 2006. *ELEMENTS OF INFORMATION THEORY*. Wiley-Interscience: Hoboken, N.J.

Crotty SM, Ortals C, Pettengill TM, Shi L, Olabarrieta M, Joyce MA, Altieri AH, Morrison E, Bianchi TS, Craft C, et al. 2020. Sea-level rise and the emergence of a keystone grazer alter the geomorphic evolution and ecology of southeast US salt marshes. *Proceedings of the National Academy of Sciences* **117** (30): 17891–17902 DOI: 10.1073/pnas.1917869117

Daubechies I. 1992. *Ten Lectures on Wavelets*. Society for Industrial and Applied Mathematics. DOI: 10.1137/1.9781611970104

Ensign SH, Piehler MF, Doyle MW. 2008. Riparian zone denitrification affects nitrogen flux through a tidal freshwater river. *Biogeochemistry* **91** (2): 133–150 DOI: 10.1007/s10533-008-9265-9

Falkowski PG, Fenchel T, Delong EF. 2008. The Microbial Engines That Drive Earth's Biogeochemical Cycles. *Science* **320** (5879): 1034–1039 DOI: 10.1126/science.1153213

Fine RA, Millero FJ. 1973. Compressibility of water as a function of temperature and pressure. *The Journal of Chemical Physics* **59** (10): 5529–5536 DOI: 10.1063/1.1679903

Foufoula-Georgiou E, Kumar P. 1994. Wavelet Analysis in Geophysics: An Introduction. In *Wavelet Analysis and Its Applications*, Foufoula-Georgiou E, , Kumar P (eds).Academic Press; 1–43. DOI: 10.1016/B978-0-08-052087-2.50007-4

Giblin A, Tobias C, Song B, Weston N, Banta G, Rivera-Monroy V. 2013. The Importance of Dissimilatory Nitrate Reduction to Ammonium (DNRA) in the Nitrogen Cycle of Coastal Ecosystems. *Oceanography* **26** (3): 124–131 DOI: 10.5670/oceanog.2013.54

Gouhier T, Grinsted A, Simko V. 2021. Biwavelet. Available at: https://cran.r-project.org/web/packages/biwavelet/biwavelet.pdf [Accessed 2 August 2021]

Grinsted A, Moore JC, Jevrejeva S. 2004. Application of the cross wavelet transform and wavelet coherence to geophysical time series. *Nonlinear Processes in Geophysics* **11** (5/6): 561–566 DOI: https://doi.org/10.5194/npg-11-561-2004

Guan K, Thompson SE, Harman CJ, Basu NB, Rao PSC, Sivapalan M, Packman AI, Kalita PK. 2011. Spatiotemporal scaling of hydrological and agrochemical export dynamics in a tile-drained Midwestern watershed. *Water Resources Research* **47** (10) DOI: 10.1029/2010WR009997

Guimond J, Tamborski J. 2021. Salt Marsh Hydrogeology: A Review. *Water* **13** (4): 543 DOI: 10.3390/w13040543

Guimond JA, Seyfferth AL, Moffett KB, Michael HA. 2020a. A physical-biogeochemical mechanism for negative feedback between marsh crabs and carbon storage. *Environmental Research Letters* **15** (3): 034024 DOI: 10.1088/1748-9326/ab60e2

Guimond JA, Yu X, Seyfferth AL, Michael HA. 2020b. Using Hydrological-Biogeochemical Linkages to Elucidate Carbon Dynamics in Coastal Marshes Subject to Relative Sea Level Rise. *Water Resources Research* **56** (2): e2019WR026302 DOI: https://doi.org/10.1029/2019WR026302

Haavisto VF. 1974. Effects of a heavy rainfall on redox potential and acidity of a waterlogged peat. *Canadian Journal of Soil Science* **54** (2): 133–135 DOI: 10.4141/cjss74-019

Haberer CM, Cirpka OA, Rolle M, Grathwohl P. 2014. Experimental Sensitivity Analysis of Oxygen Transfer in the Capillary Fringe. *Groundwater* **52** (1): 37–49 DOI: 10.1111/gwat.12028

Hamersley MR, Howes BL. 2005. Coupled nitrification–denitrification measured in situ in a Spartina alterniflora marsh with a 15NH4+ tracer. *Marine Ecology Progress Series* **299**: 123–135 DOI: 10.3354/meps299123

Hammer DA, Bastian RK. 1989. Wetlands Ecosystems: Natural Water Purifiers? In *Constructed Wetlands for Wastewater Treatment*CRC Press.

Hariprasath S, Mohan V. 2008. Biometric personal identification based on iris recognition using complex wavelet transforms. In *2008 International Conference on Computing, Communication and Networking*1–5. DOI: 10.1109/ICCCNET.2008.4787736

Henderson RD, Day-Lewis FD, Lane JW, Harvey CF, Liu L. 2008. Characterizing Submarine Groundwater Discharge Using Fiber-Optic Distributed Temperature Sensing and Marine

Electrical Resistivity. In *Symposium on the Application of Geophysics to Engineering and Environmental Problems 2008*Environment and Engineering Geophysical Society; 775–785. DOI: 10.4133/1.2963319

Joye SB, Hollibaugh JT. 1995. Influence of Sulfide Inhibition of Nitrification on Nitrogen Regeneration in Sediments. *Science* **270** (5236): 623–625

Kantelhardt JW, Rybski D, Zschiegner SA, Braun P, Koscielny-Bunde E, Livina V, Havlin S, Bunde A. 2003. Multifractality of river runoff and precipitation: comparison of fluctuation analysis and wavelet methods. *Physica A: Statistical Mechanics and its Applications* **330** (1): 240–245 DOI: 10.1016/j.physa.2003.08.019

Koop-Jakobsen K, Wenzhöfer F. 2015. The Dynamics of Plant-Mediated Sediment Oxygenation in Spartina anglica Rhizospheres—a Planar Optode Study. *Estuaries and Coasts* **38** (3): 951–963 DOI: 10.1007/s12237-014-9861-y

Kumar P, Foufoula-Georgiou E. 1997. Wavelet analysis for geophysical applications. *Reviews of Geophysics* **35** (4): 385–412 DOI: 10.1029/97RG00427

Kvålseth TO. 2017. On Normalized Mutual Information: Measure Derivations and Properties. *Entropy* **19** (11): 631 DOI: 10.3390/e19110631

Labat D, Ronchail J, Callede J, Guyot JL, Oliveira ED, Guimarães W. 2004. Wavelet analysis of Amazon hydrological regime variability. *Geophysical Research Letters* **31** (2) DOI: 10.1029/2003GL018741

Lahiri C, Davidson GR. 2020. Heterogeneous oxygenation of wetland soils with increasing inundation: Redox potential, water depth, and preferential flow paths. *Hydrological Processes*: hyp.13654 DOI: 10.1002/hyp.13654

Liu W, Maxwell B, Birgand F, Youssef M, Chescheir G, Tian S. 2020. Multipoint High-Frequency Sampling System to Gain Deeper Insights on the Fate of Nitrate in Artificially Drained Fields. *Journal of Irrigation and Drainage Engineering* **146** (1): 06019012 DOI: 10.1061/(ASCE)IR.1943-4774.0001438

Mallat S. 1999. *A Wavelet Tour of Signal Processing: The Sparse Way (Wavelet Analysis & Its Applications)*. Academic Press: Burlington, MA 01803, USA.

Maraun D, Kurths J. 2004. Cross wavelet analysis: significance testing and pitfalls. *Nonlinear Processes in Geophysics* **11** (4): 505–514 DOI: 10.5194/npg-11-505-2004

Martínez B, Gilabert MA. 2009. Vegetation dynamics from NDVI time series analysis using the wavelet transform. *Remote Sensing of Environment* **113** (9): 1823–1842 DOI: 10.1016/j.rse.2009.04.016

Meinzer OE. 1927. Plants as Indicators of Groundwater. Scientific Investigations Report. United States Geological Survey, Washington, DC. Available at: https://pubs.usgs.gov/wsp/0577/report.pdf [Accessed 26 January 2022]

Menció A, Casamitjana X, Mas-Pla J, Coll N, Compte J, Martinoy M, Pascual J, Quintana XD. 2017. Groundwater dependence of coastal lagoons: The case of La Pletera salt marshes (NE Catalonia). *Journal of Hydrology* **552**: 793–806 DOI: 10.1016/j.jhydrol.2017.07.034

Messer TL, Birgand F, Burchell MR. 2019. Diel fluctuations of high level nitrate and dissolved organic carbon concentrations in constructed wetland mesocosms. *Ecological Engineering* **133**: 76–87 DOI: 10.1016/j.ecoleng.2019.04.027

Minamikawa K, Sakai N. 2007. Soil carbon budget in a single-cropping paddy field with rice straw application and water management based on soil redox potential. *Soil Science and Plant Nutrition* **53** (5): 657–667 DOI: 10.1111/j.1747-0765.2007.00172.x

Murphy AE, Bulseco AN, Ackerman R, Vineis JH, Bowen JL. 2020. Sulphide addition favours respiratory ammonification (DNRA) over complete denitrification and alters the active microbial community in salt marsh sediments. *Environmental Microbiology* **22** (6): 2124–2139 DOI: 10.1111/1462-2920.14969

NERR. 2021. NOAA National Estuarine Research Reserve System (NERRS). System-wide Monitoring Program. Data accessed from the NOAA NERRS Centralized Data Management Office website: www.nerrsdata.org

Nezlin NP, Kamer K, Hyde J, Stein ED. 2009. Dissolved oxygen dynamics in a eutrophic estuary, Upper Newport Bay, California. *Estuarine, Coastal and Shelf Science* **82** (1): 139–151 DOI: 10.1016/j.ecss.2009.01.004

Nivala J, Murphy C, Freeman A. 2020. Recent Advances in the Application, Design, and Operations & Maintenance of Aerated Treatment Wetlands. *Water* **12** (4): 1188 DOI: 10.3390/w12041188

Orduña-Gaytán F, Vallejo-Cantú NA, Alvarado-Vallejo A, Rosas-Mendoza ES, Sandoval-Herazo LC, Alvarado-Lassman A. 2022. Evaluation of the Removal of Organic Matter and Nutrients in the Co-Treatment of Fruit and Vegetable Waste Using a Bioreactor-Constructed Wetlands System. *Processes* **10** (2): 278 DOI: 10.3390/pr10020278

Osif TL. 1988. The Effects of Salt, Gas, Temperature, and Pressure on the Compressibility of Water. *SPE Reservoir Engineering* **3** (01): 175–181 DOI: 10.2118/13174-PA

Partal T. 2012. Wavelet analysis and multi-scale characteristics of the runoff and precipitation series of the Aegean region (Turkey). *International Journal of Climatology* **32** (1): 108–120 DOI: 10.1002/joc.2245

Petersen NR-, Rysgaard S, Nielsen LP, Revsbech NP. 1994. Diurnal variation of denitrification and nitrification in sediments colonized by benthic microphytes. *Limnology and Oceanography* **39** (3): 573–579 DOI: 10.4319/lo.1994.39.3.0573

Quiroz R, Yarlequé C, Posadas A, Mares V, Immerzeel WW. 2011. Improving daily rainfall estimation from NDVI using a wavelet transform. *Environmental Modelling & Software* **26** (2): 201–209 DOI: 10.1016/j.envsoft.2010.07.006

R Core Team. 2019. *R: A Language and Environment for Statistical Computing*. R Fundation for Statistical Computing. Available at: https://www.R-project.org/

Reading MJ, Santos IR, Maher DT, Jeffrey LC, Tait DR. 2017. Shifting nitrous oxide source/sink behaviour in a subtropical estuary revealed by automated time series observations. *Estuarine, Coastal and Shelf Science* **194**: 66–76 DOI: 10.1016/j.ecss.2017.05.017

Sarkar S, Pandey B. 2020. A study on the statistical significance of mutual information between morphology of a galaxy and its large-scale environment. *Monthly Notices of the Royal Astronomical Society* **497** (4): 4077–4090 DOI: 10.1093/mnras/staa2236

Shannon CE, Weaver W. 1949. The mathematical theory of communication

Søndergaard M. 2009. Redox Potential. In *Encyclopedia of Inland Waters*, Likens GE (ed.).Academic Press: Oxford; 852–859. DOI: 10.1016/B978-012370626-3.00115-0

Steinmuller HE, Chambers LG. 2019. Characterization of coastal wetland soil organic matter: Implications for wetland submergence. *Science of The Total Environment* **677**: 648–659 DOI: 10.1016/j.scitotenv.2019.04.405

Taniguchi M. 2000. Evaluations of the saltwater-groundwater interface from borehole temperature in a coastal region. *Geophysical Research Letters* **27** (5): 713–716 DOI: 10.1029/1999GL002366

The MathWorks I. 2021. MATLAB Wavelet Toolbox. MathWorks, Inc.: Natick, Massachusetts, US.

Torrence C, Compo GP. 1998. A Practical Guide to Wavelet Analysis. *Bulletin of the American Meteorological Society* **79** (1): 18

Turner IL, Coates BP, Acworth RI. 1997. Tides, Waves and the Super-elevation of Groundwater at the Coast. *Journal of Coastal Research* **13** (1): 46–60

Valiela I, Cole ML. 2002. Comparative Evidence that Salt Marshes and Mangroves May Protect Seagrass Meadows from Land-derived Nitrogen Loads. *Ecosystems* **5** (1): 92–102 DOI: 10.1007/s10021-001-0058-4

Van Dyke E, Wasson K. 2005. Historical ecology of a central California estuary: 150 years of habitat change. *Estuaries* **28** (2): 173–189 DOI: 10.1007/BF02732853

Venkatesh S, Arora B, Dwivedi D, Vezhapperambu S, Ramesh MV. 2021. Temporal Variability of Water Quality Parameters at the Elkhorn Slough Estuary using Wavelets. In *2021 6th International Conference for Convergence in Technology (I2CT)*1–5. DOI: 10.1109/I2CT51068.2021.9418159

Vorenhout M, van der Geest HG, Hunting ER. 2011. An improved datalogger and novel probes for continuous redox measurements in wetlands. *International Journal of Environmental Analytical Chemistry* **91** (7–8): 801–810 DOI: 10.1080/03067319.2010.535123

Vorenhout M, van der Geest HG, van Marum D, Wattel K, Eijsackers HJP. 2004. Automated and Continuous Redox Potential Measurements in Soil. *Journal of Environmental Quality* **33** (4): 1562–1567 DOI: 10.2134/jeq2004.1562

Wallace CD, Soltanian MR. 2021. Underlying riparian lithology controls redox dynamics during stage-driven mixing. *Journal of Hydrology* **595**: 126035 DOI: 10.1016/j.jhydrol.2021.126035

Wallace CD, Sawyer AH, Barnes RT. 2019. Spectral analysis of continuous redox data reveals geochemical dynamics near the stream–aquifer interface. *Hydrological Processes* **33** (3): 405–413 DOI: 10.1002/hyp.13335

Wankel SD, Germanovich LN, Lilley MD, Genc G, DiPerna CJ, Bradley AS, Olson EJ, Girguis PR. 2011. Influence of subsurface biosphere on geochemical fluxes from diffuse hydrothermal fluids. *Nature Geoscience* **4** (7): 461–468 DOI: 10.1038/ngeo1183

Wankel SD, Kendall C, Paytan A. 2009. Using nitrate dual isotopic composition (δ^{15}N and δ^{18}O) as a tool for exploring sources and cycling of nitrate in an estuarine system: Elkhorn Slough, California. *Journal of Geophysical Research* **114** (G1): G01011 DOI: 10.1029/2008JG000729

Wong LS, Hashim R, Ali FH. 2009. A Review on Hydraulic Conductivity and Compressibility of Peat. *Journal of Applied Sciences* **9** (18): 3207–3218 DOI: 10.3923/jas.2009.3207.3218

Woolfolk A, Labadie Q. 2012. The significance of pickleweed-dominated tidal salt marsh in Elkhorn Slough, California: A literature review. Technical Report Series. Elkhorn Slough.

Xie T, Li S, Cui B, Bai J, Wang Q, Shi W. 2019. Rainfall variation shifts habitat suitability for seedling establishment associated with tidal inundation in salt marshes. *Ecological Indicators* **98**: 694–703 DOI: 10.1016/j.ecolind.2018.11.056

Zbili M, Rama S. 2021. A Quick and Easy Way to Estimate Entropy and Mutual Information for Neuroscience. *Frontiers in Neuroinformatics* **15**: 25 DOI: 10.3389/fninf.2021.596443

Zhang X, Zhao X-M, He K, Lu L, Cao Y, Liu J, Hao J-K, Liu Z-P, Chen L. 2012. Inferring gene regulatory networks from gene expression data by path consistency algorithm based on conditional mutual information. *Bioinformatics* **28** (1): 98–104 DOI: 10.1093/bioinformatics/btr626

Zheng Y, Hou L, Liu M, Liu Z, Li X, Lin X, Yin G, Gao J, Yu C, Wang R, et al. 2016. Tidal pumping facilitates dissimilatory nitrate reduction in intertidal marshes. *Scientific Reports* **6** (1): 21338 DOI: 10.1038/srep21338

TABLES

Table 1. Summary of periods (frequencies) at which significant powers in the Eh wavelet occur.

Significant Periods

Depth (cm)	***Lower Marsh***	***Middle Marsh***	***Upper Marsh***
10	1:64 h & > 512 h	12h and 24h (tidal frequencies)	12h and 24h (tidal frequencies), 355h and 708h (lunar cycle)
30	12h and 24h (tidal frequencies)	24h (daily cycle)	12h and 24h (tidal frequencies)
50	12h and 24h (tidal frequencies), 355h and 708h (lunar cycle)	12h and 24h (tidal frequencies), 355h and 708h (lunar cycle)	12h and 24h (tidal frequencies)

FIGURE LEGENDS

Figure 1. A) Map of Elkhorn Slough with the extent of wetlands outlined in light blue. The black star marks the location of the study transect. B) Map view of the experimental transect showing the location of the upland monitoring piezometer in relation to the salt marsh transect. C) Labeled diagram of the redox probe and reference electrode used for this project. D) Illustration of the experimental transect showing the spatial distribution of the redox (Eh) probes and observation wells with a contour plot overlay of sediment bulk density across the salt marsh. The darker the colors in the contour plot, the greater the bulk density (highest around 30 cm at all three marsh positions).

Figure 2. Redox potential (Eh) contour graphs across the experimental transect. The grey, dashed lines at 10, 30 and 50 cm indicate the Eh probe's depth, the values in between are linearly interpolated. Soil bulk density at each marsh position is shown to the right of each contour plot. Precipitation time series for the studied period is shown above the Eh profile to illustrate the timing of storm events. The time series corresponding to this contour plot can be found as supporting information S2.

Figure 3. Continuous wavelet spectrum and global wavelet spectrum of Eh time series between March 2020 and February 2021. In the wavelet spectrum, the shaded regions signify the cone of influence. The color bar signifies the strength of power in the wavelet spectrum. Areas surrounded by the black polygons display significant powers (within 95% significance level). In the global wavelet spectrum, the red-dashed line is the 95% significance level using a red-noise background spectrum. The shaded area in the 30 cm depth of the lower marsh (bottom center panel) marks the time of a precipitation event studied in detail in Figure 5.

Figure 4. Mutual information between Eh time series and other hydroclimatic parameters used to explore Eh's temporal variability. All the relationships between Eh and the parameters shown in the figure are statistically significant (p-value <0.0001). The mutual information values are normalized by the Entropy of each individual signal.

Figure 5. Multilevel decomposition of Eh for the 10 cm, 30 cm, and 50 cm depths in the lower marsh position between January 20th and February 10th, 2021 (marked in Figure 3 by a shaded rectangle). ***A****) shows the Eh approximate coefficients at 16 h, hourly precipitation (P), and hourly evapotranspiration (ET).* ***B****) shows local subsurface water level, air temperature, water temperature, and regional terrestrial groundwater level.* ***C****) shows the detailed components of Eh at dyadic scales of 2 (d1), 4 (d2), 8 (d3), 16(d4), and 32 (d5). The shaded region marks a precipitation event that occurred in the area in late January. The dashed gray line in* ***B****) marks the elevation (amsl) of the salt marsh. The vertical dashed gray lines mark the beginning of every new day (midnight).*

Figure 6. Cross wavelet analysis of subsurface water level and Eh signals at the 30 cm depth in the lower marsh position. The figure shows the modulus (power) and phase (angle in radians) of the wavelet cross-spectrum in the top and bottom panels, respectively. The power plot indicates higher coherences with blue and green colors while low coherence is illustrated by gray colors. In the phase shift, the 0 radian value indicates that the two time series are in phase while +3 radians and -3 radians indicate anti-phase (Note that the color scale actually goes from $-\pi$ to $+\pi$). Arrows pointing towards the right indicate that the time series are in phase, arrows pointing to the left indicate that the two time series are anti-phase, arrows pointing downward explain that the subsurface water level is leading, and arrows pointing upward indicate that the subsurface water level is lagging.

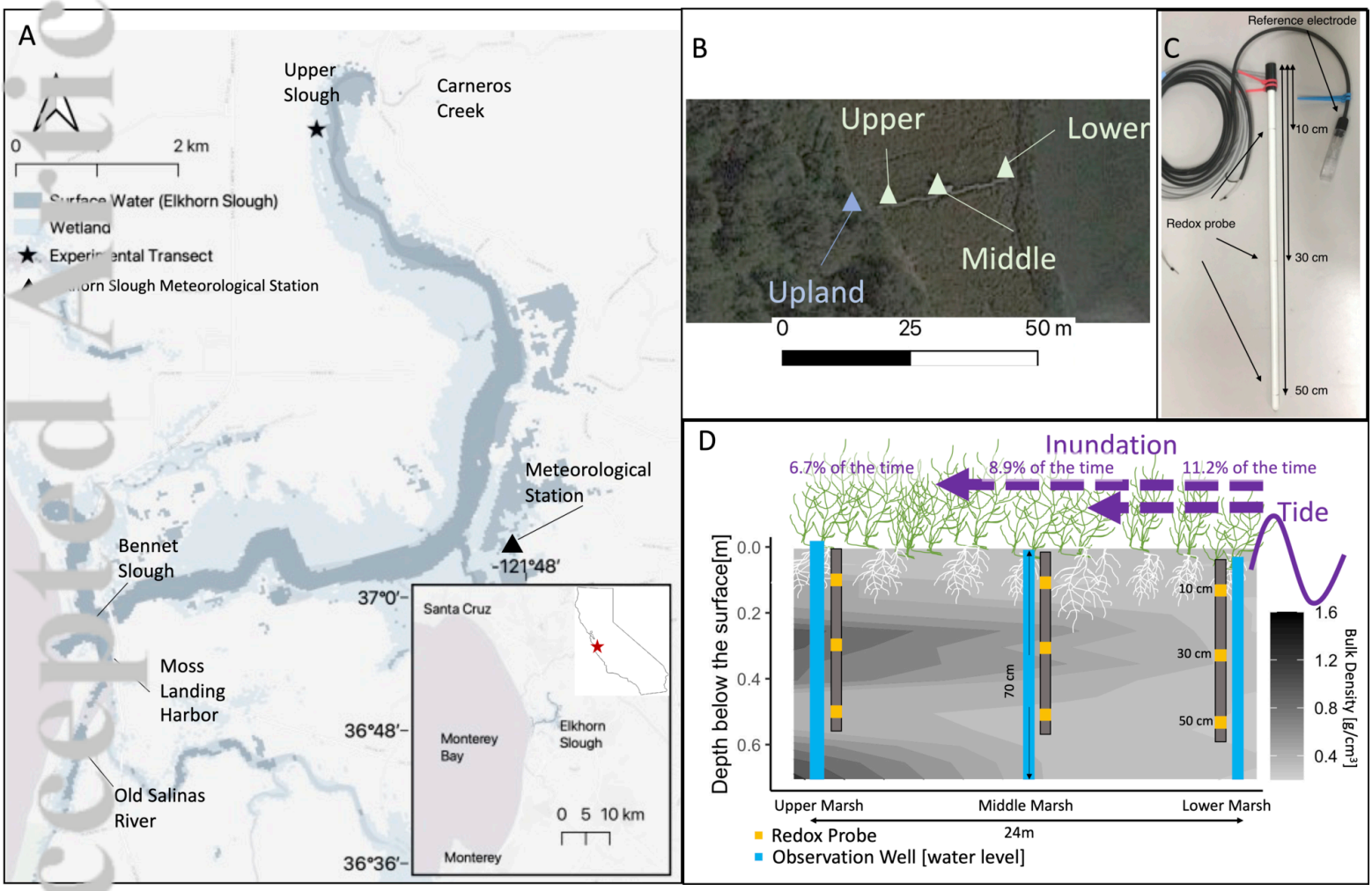

Fig1.tiff

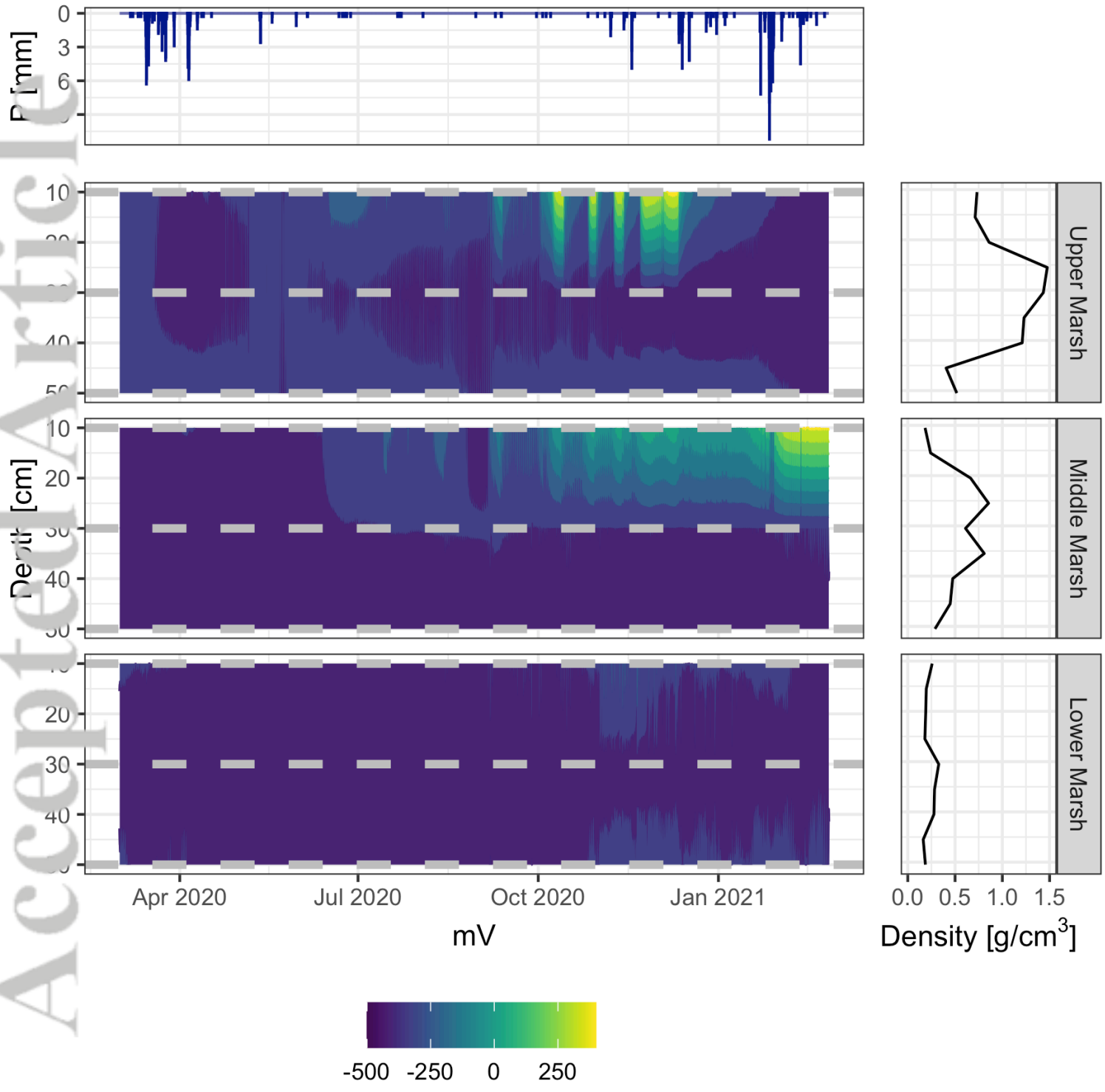

Fig2.tiff

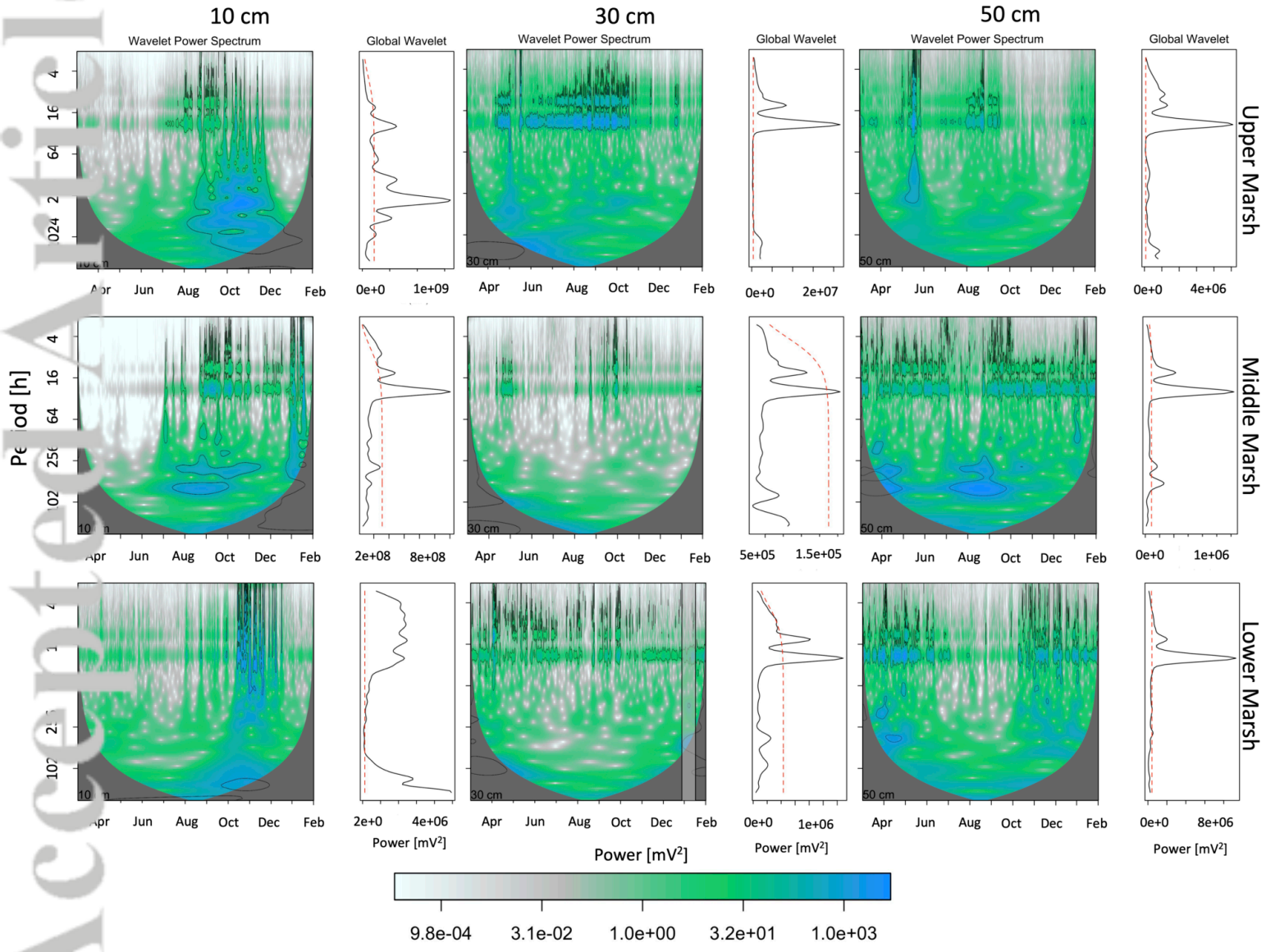

Fig3.tiff

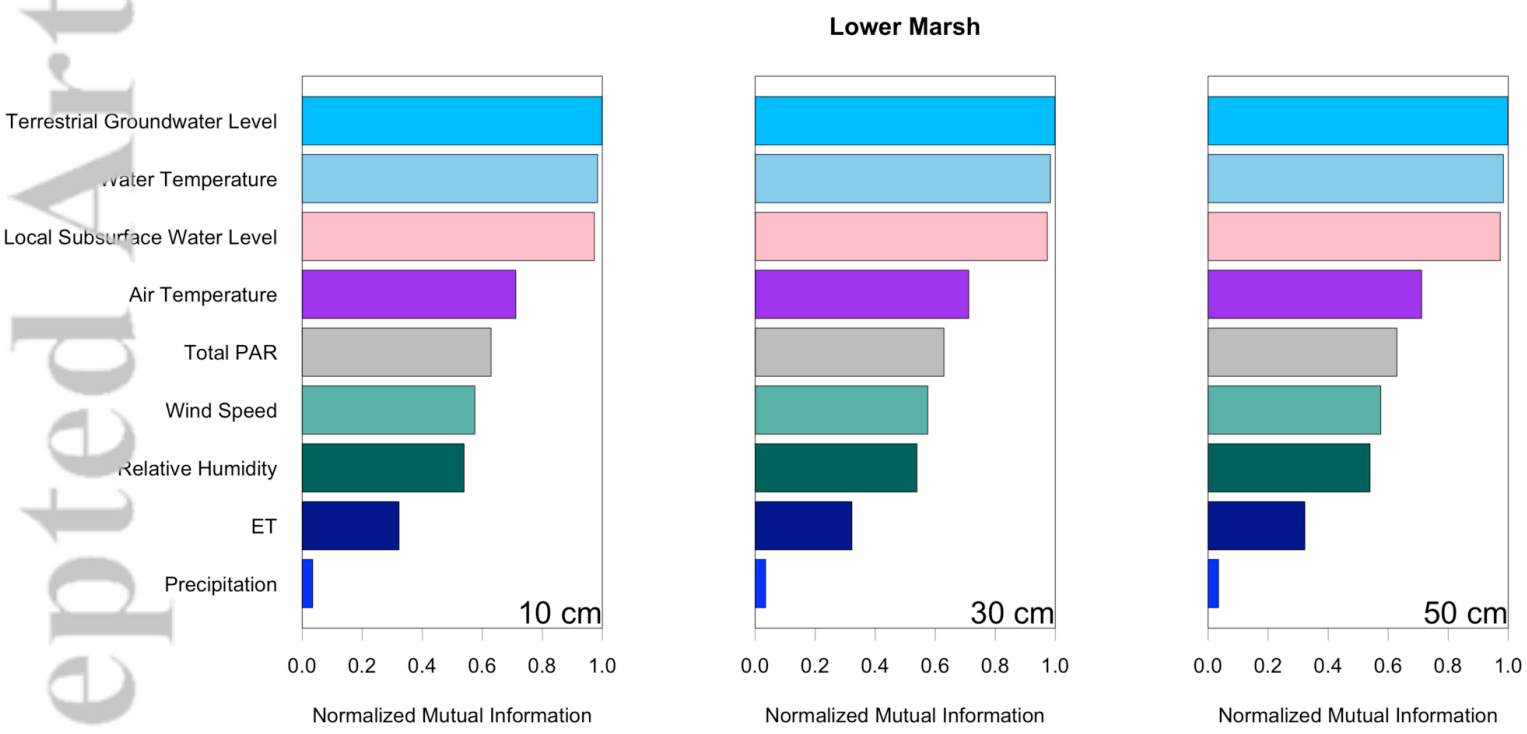

Fig4.png

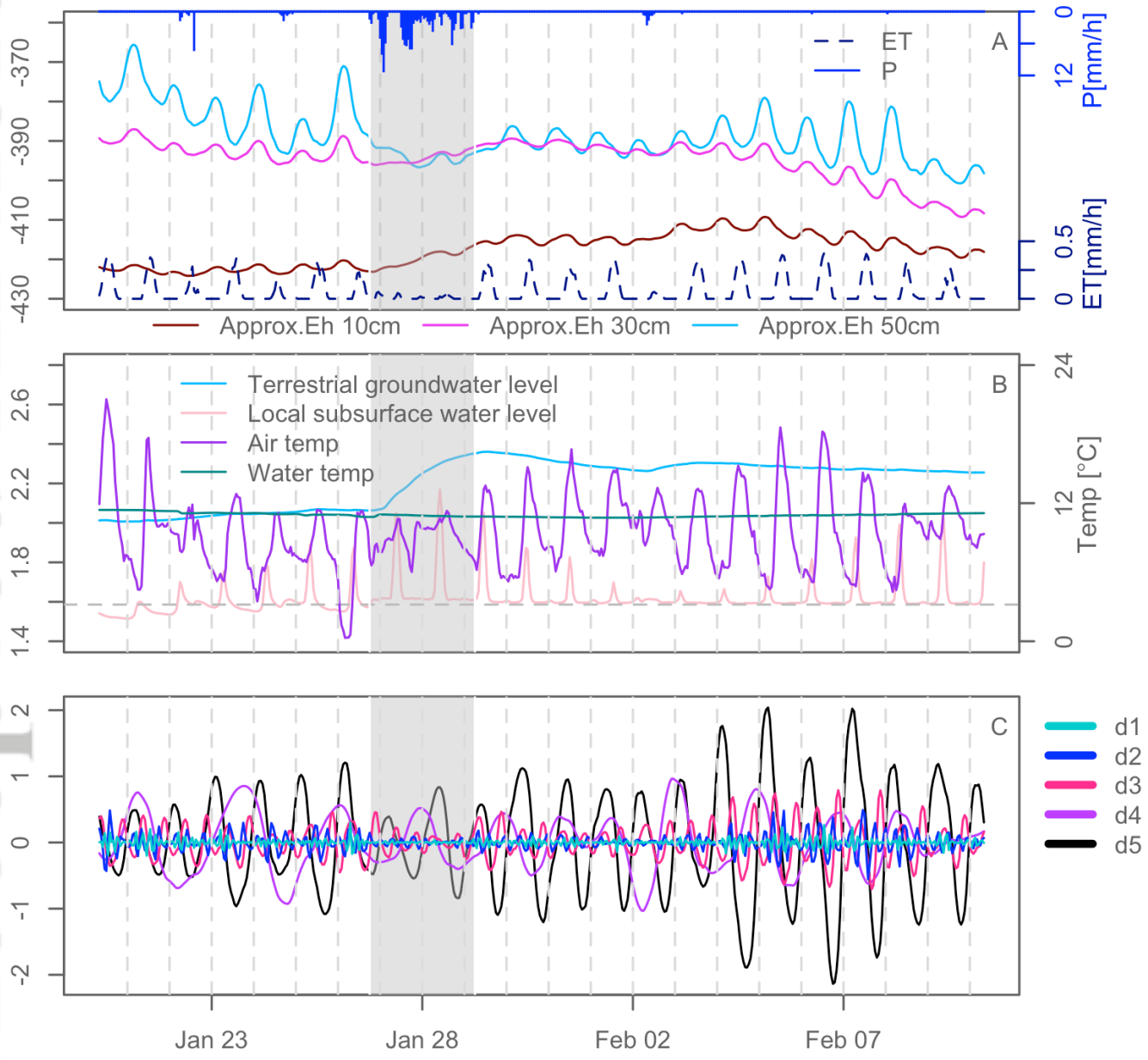

Fig5.tiff

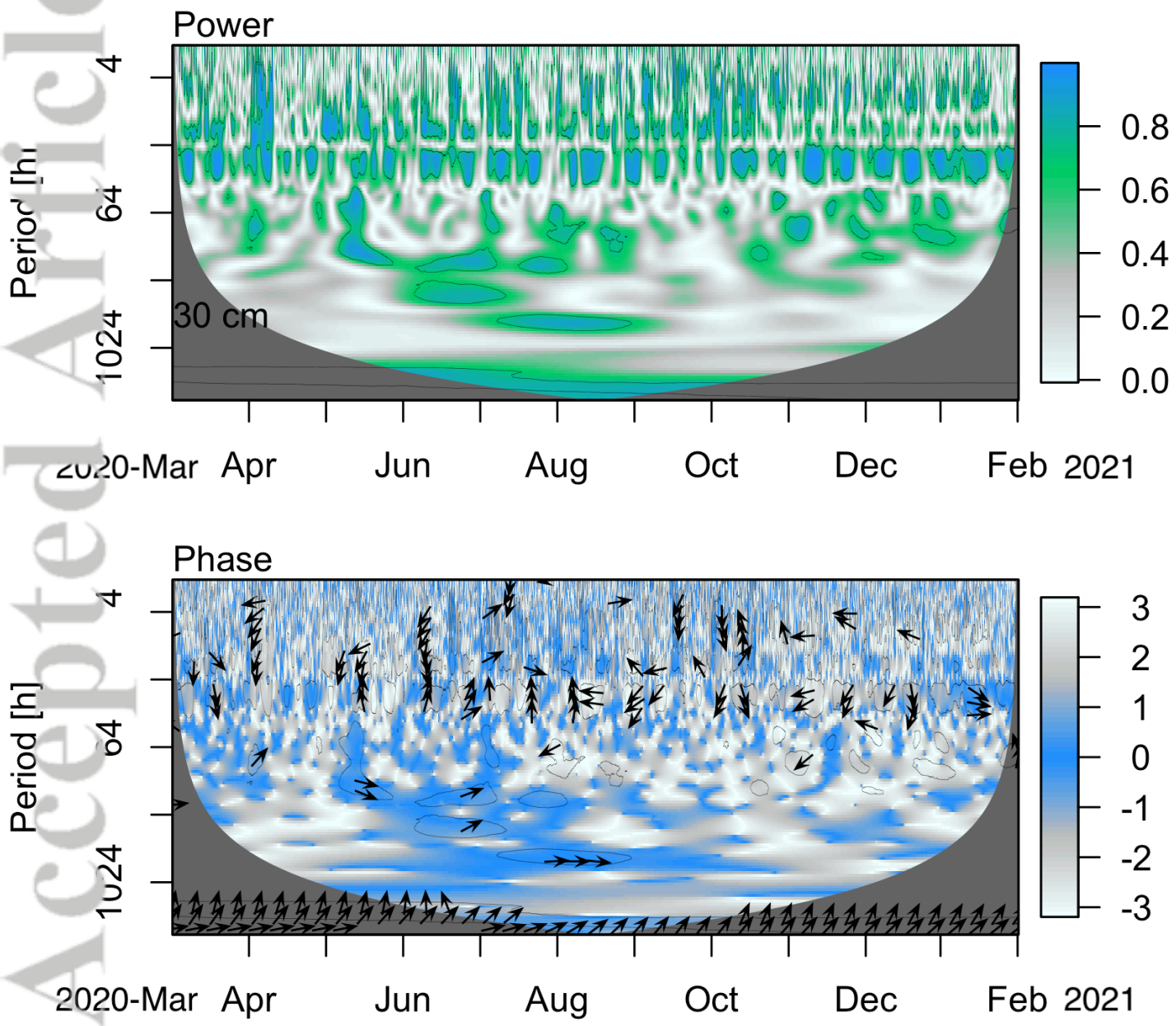

Fig6.tiff